Bulletin of the Seismological Society of America. Vol. 65, No. 5, pp. 1059–1071. October 1975

SURFACE STRONG MOTION ASSOCIATED WITH A STICK-SLIP EVENT IN A FOAM RUBBER MODEL OF EARTHQUAKES

By Ralph J. Archuleta and James N. Brune

ABSTRACT

In this paper, we present and interpret dynamic displacement data for a stick-slip event in a foam rubber model of earthquake faulting. Static displacement data are used to infer the stress drop of about 0.016 μ, where μ is the shear modulus. The rupture velocity 0.7 β, where β is the shear-wave speed, is also inferred from the data. The observed particle displacement and particle velocity data are compared with analytical and numerical predictions. Doppler focusing of energy by rupture propagation is clearly observed. No large transverse displacement pulse such as that observed at Station 2 of the Parkfield earthquake is observed. In addition to its value for testing analytical and numerical predictions, the laboratory model provides much needed information on the distribution of strong ground motion in the neighborhood of a fault and thus helps in the problem of microzonation for earthquakes.

Introduction

During the past decade, numerous authors have attempted to solve for the elastodynamic displacement field which results from the sudden release of tractions over a prescribed plane embedded in either a half-space or a full space. A model of stress relaxation over a plane which closely approximates our present concept of shallow earthquakes was studied by Kostrov (1964) who solved the problem of a self-similar, circular fault plane in a three-dimensional (3-D) full space. Kostrov (1964) calculated explicitly the discontinuity in displacement on the fault plane as a function of time. Papers by Burridge and Willis (1969), Richards (1973), Burridge (1973) and Burridge and Levy (1974) extend the analysis of self-similar solutions for elliptical cracks in three dimensions. Analytical solutions for cracks which stop are limited to the special case of anti-plane strain shear cracks (Kostrov, 1966; Burridge and Halliday, 1971). A root-mean-square approximation was given by Brune (1970).

An alternative to the analytical techniques for solving the stress relaxation problem is the numerical approach, using either finite element or finite difference schemes to allow directly for the equations and boundary conditions. Dieterich (1973) used a finite element technique while Hanson, Sanford and Schaffer (1974) and Madariaga (1974) have solved the equations of motion and boundary conditions using finite difference schemes.

It would be convenient to measure directly the displacement field during the sudden release of tractions in the case of an earthquake. The unpredictability of earthquakes, both in time and space, has prevented acquisition of such data to date; although with many more strong-motion seismographs being employed, we will certainly have better estimates in coming years. Fortunately, laboratory models can be constructed to serve as analogs of the earthquake process. One such model was devised by Brune (1973) who used it to measure the displacement-time function near the center of the fault trace during stick-slip events. Encouraged by these single point observations, we decided to

attempt to measure the entire surface elastodynamic displacement field during a stick-slip event.

Experimental Procedure and Results

We have taken a block of polyurethene elastomer (foam rubber) 0.76 by 0.76 by 0.38 m as our analog of a homogeneous, isotropic, elastic medium. In the center of one of the square faces of the block, we made a semicircular cut, 80 mm in radius, to simulate a pre-existing strike-slip fault which intersects a free surface (Figure 1). By gluing $\frac{3}{4}$-in plywood to opposite sides of the foam rubber block, we are then able to apply uniform normal and shear stress using the apparatus described by Brune (1973). The shear-wave speed in the block is 30.33 mm/msec and the compression-wavespeed is 52.50 mm/msec. The model size and the wave speeds are such that the dynamic processes on the fault

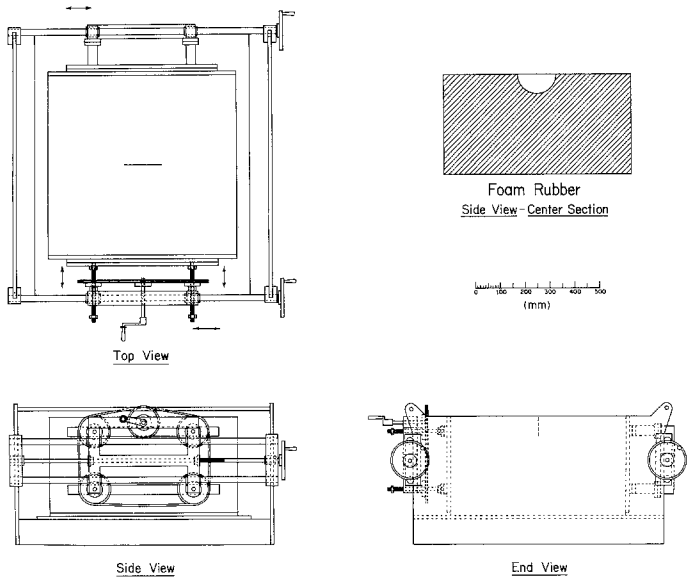

FIG. 1. Illustration of machine by which we apply uniform normal and shear stress to rectangular block of foam rubber. Fault trace is shown in middle of block.

surface terminate before any reflected pulses from the sides of the block return to contaminate the measurements.

In order to initiate a stick-slip event, we first fix the normal stress at some constant value. Then we slowly turn the gears attached to the plywood (Figure 1) and displace the outer boundaries of the foam block, thereby increasing the shearing tractions on the sides of the fault until a stick-slip event occurs. Approximately 1 sec before the stick-slip event, the camera is turned on to record the event. Because of the reproducibility of the experiment, we can estimate the time of initiation to within one or two full turns of the gears. However, because we are turning the gears slowly, the exposure time of the film (about 4 sec) may elapse before the stick-slip event occurs. (The results presented in this paper were obtained after four prior attempts.)

Mounted directly above the surface of the foam rubber is a Fastax camera capable of filming at a rate of up to 5500 frames/sec. The surface of the foam is marked with black beads about $\frac{1}{2}$ mm in diameter. The beads are inserted into the small voids of the foam

rubber. Approximately 10 mm above the free surface, and parallel to it, is an isolated square wire grid with line spacing of about 5 mm. The intersections of this grid serve as stationary reference points relative to which absolute displacements of the beads are measured. Points on enlarged frames of film are digitized to obtain the displacement-time history (using a Benson-Lehner digitizer which digitizes 500 counts/25.4 mm).

For this particular experiment, the frame rate was 4286 frames/sec or 1 frame per 0.233 msec. Thus, the shortest resolvable period is 0.233×10^{-3} sec which corresponds to a wavelength for a traveling shear wave of about 7 mm, much larger than the voids in the foam rubber and the marking beads. The magnitude of the displacements, the

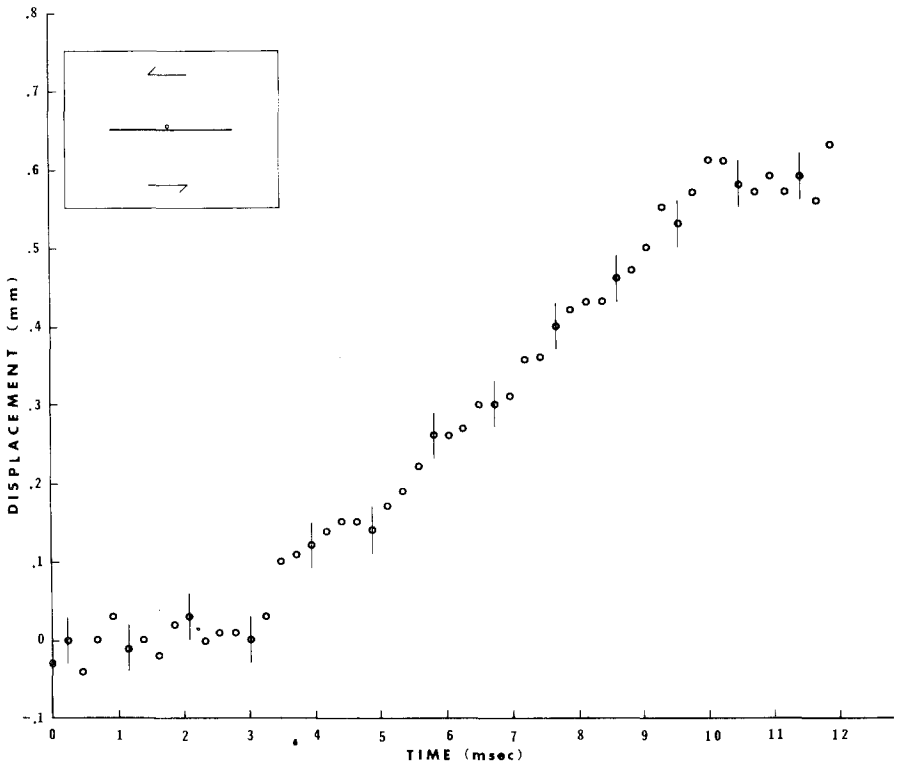

FIG. 2. Time history of displacement for a point located near the center of the fault trace.

coarseness of the film, and the camera's field of view limited this experiment to an area 260 by 120 mm centered on the fault trace.

In the following discussion, unless specifically stated otherwise, displacement refers to that component of displacement parallel to the fault trace. An example of the measurements for a point located near the center of the fault trace is shown in Figure 2. The *insert* in the *upper left-hand corner* indicates the position of the measuring point relative to the fault trace; this point is 68 mm along the fault. Error bars have been drawn through each one-fifth point. The error bars represent two standard deviations as determined from successive measurements of the enlarged frames of film. The discrete time interval reflects the frame rate for this experiment. The origin of the time axis is only relative.

Some of the more apparent features of this graph are; first, there is a static or permanent offset of 0.6 mm; second, the particle velocity has a definite change around 4 msec; and third, the time for the particle to reach its static value (about 7 msec) is

longer than the time for an S-wave to traverse a radius of the fault (about 2.67 msec). Comparison of Figure 2 with results of Brune (1973) for a similar point on the fault trace shows that this particular stick-slip event produced a displacement-time history which is similar in rise time and shape to many of the displacement-time histories which Brune observed for a point near the center of the fault trace.

From our measurements of the static offsets we were able to determine the stress drop by two independent methods. First, we averaged the static displacements of 15 points adjacent to the fault trace, obtaining an average value of absolute displacement ($\bar{u}$) of

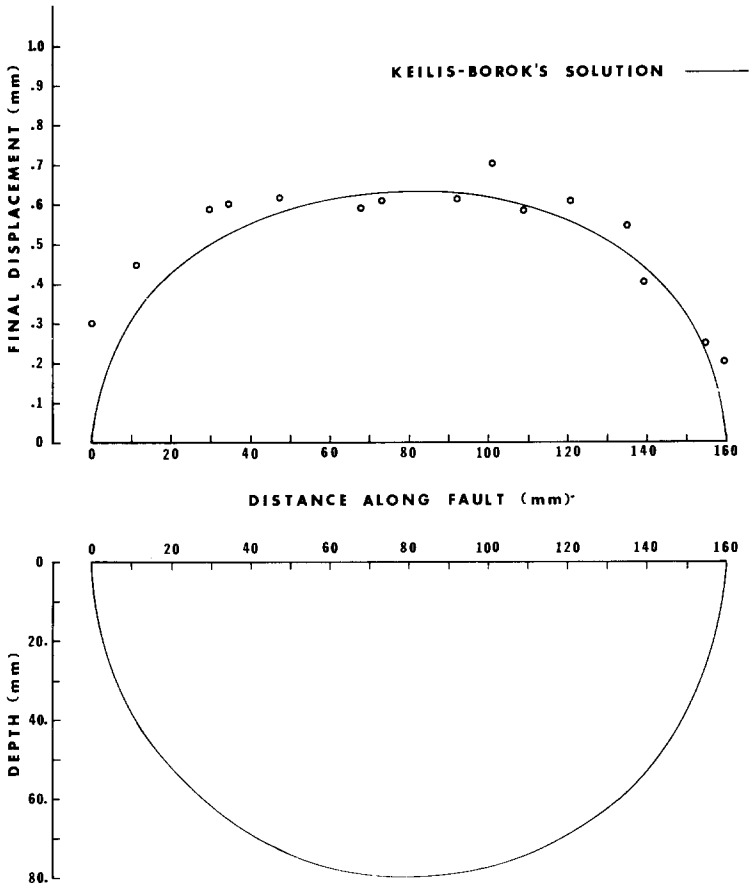

FIG. 3. Comparison of static values of displacement from this experiment with analytic solution of Keilis–Borok for points along the fault trace. Also shown is the side view of the semicircular fault plane.

0.48 mm. This was used to estimate stress drop from the formula given by Keilis-Borok (1959) for a circular fault. (Since the ratio of the P-wave speed to the S-wave speed is approximately $\sqrt{3}$, we will assume Lamé constant λ equals the shear modulus μ in our calculations.)

$$\bar{u} = \frac{8}{7\pi} \frac{\Delta\tau}{\mu} r_0 \tag{1}$$

where $\Delta\tau$ is the change in stress, and r_0 is the radius of a circular fault (80 mm). This yields a stress drop of 0.0165 μ.

We checked the result using the expression for the displacement as a function of distance along any radius of the fault (Keilis-Borok, 1959)

$$u(r) = \frac{12}{7\pi}\frac{\Delta\tau}{\mu}(r_0^2 - r^2)^{1/2}. \tag{2}$$

Using this expression along with the ratio of $\Delta\tau/\mu$ equal to 0.0165 we computed the analytical static displacements to be compared with our measured values. This comparison

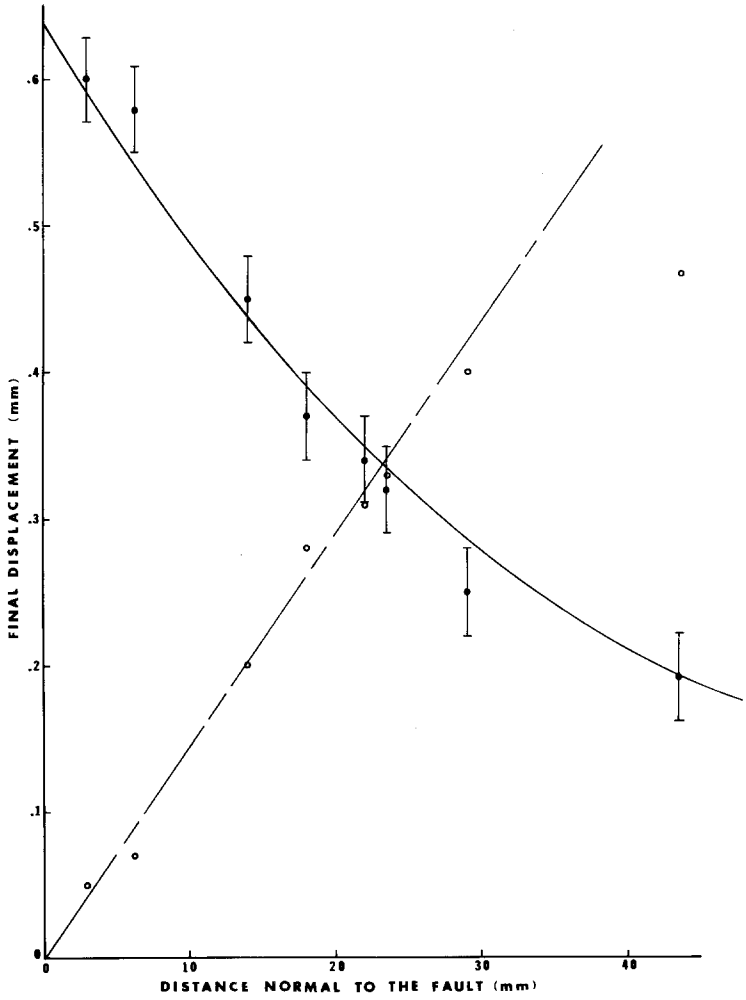

FIG. 4. The solid circles are the static values of displacement measured as a function of distance normal to the center of the fault trace. The solid line is Neuber's analytical solution. The open circles are values obtained by subtracting the displacement values from 0.65 mm. The slope of the dashed line (the strain drop) is 0.015.

is shown in Figure 3. Since our points do not lie precisely on the fault trace, we would not expect exact agreement, particularly at the end points. The fit confirms the estimate of stress drop of about 0.016 μ.

The second method of estimating stress drop involves measurements of static displacements along a line normal to the center of the fault trace. One can see that the displacements along the fault trace are rather constant near the center. Thus, we do not expect any gross errors resulting from our points being somewhat off the center line.

The measured static displacements as a function of distance normal to the fault trace are shown as the points in Figure 4 (with error bars). We extrapolated the measurements to the fault trace to obtain an approximate displacement of 0.65 mm. Then, following the procedure used by H. F. Reid (1910, 1969) in his study of the 1906 San Francisco earth-

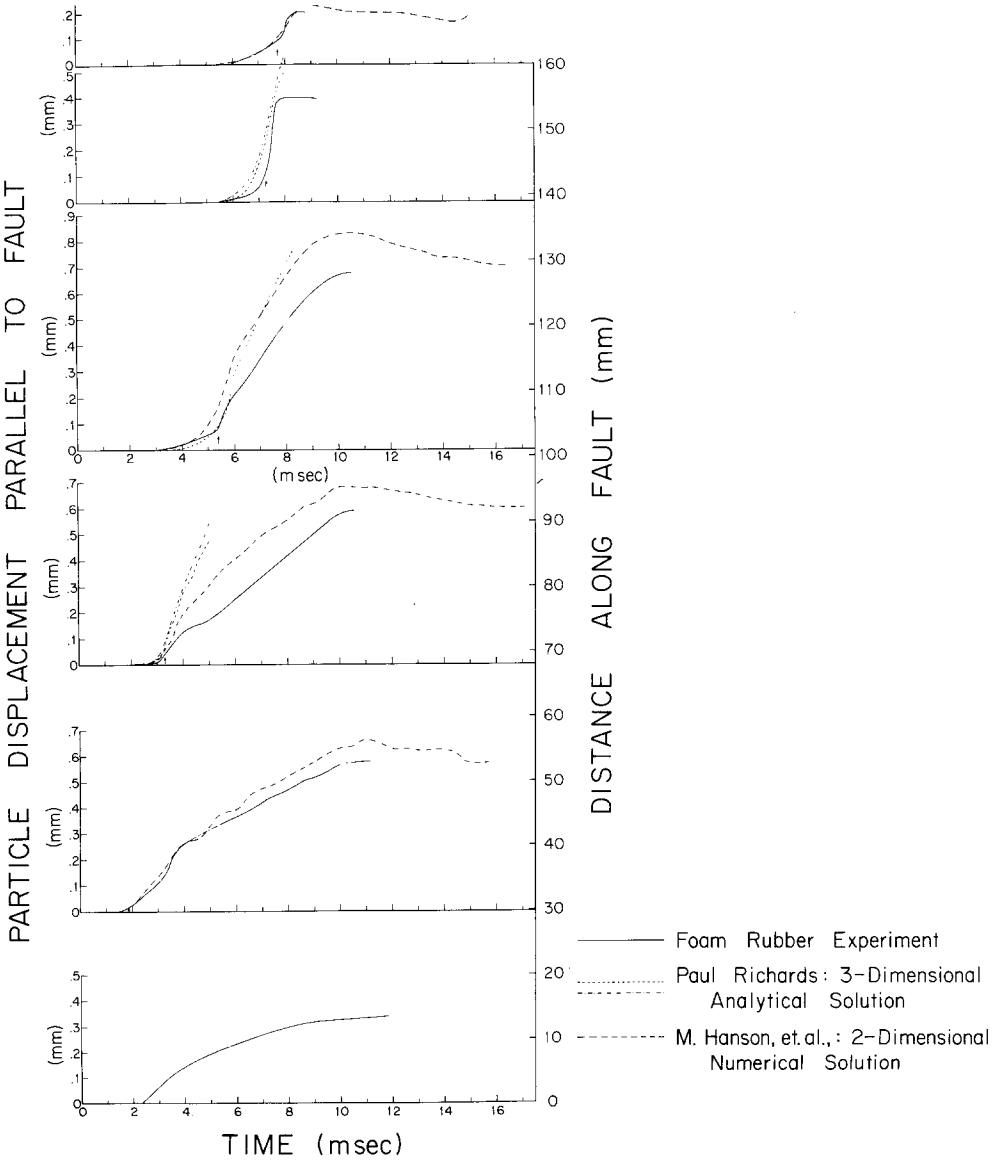

FIG. 5. Time history of displacement of six points for different positions along the fault trace from foam experiment. Also shown are analytical results from Richards and numerical results from Hanson *et al.* (1974) for dynamic shear fracture. The surface rupture originated between 30 and 40 mm along the fault, then propagated bilaterally to both ends of the fault.

quake, we subtracted the measured values of displacement from the displacement at the fault trace. This yields the values shown by open circles in Figure 4. The slope of the line passing through the open circles is 0.015 (corresponding to a stress drop of 0.015 μ). Within the accuracy of measurement, this is in good agreement with the previous estimate.

In Figure 4, the solid line is Neuber's (1958) analytical solution for amplitude of static displacement as a function of distance normal to a circular fault with a radius of 80 mm (the same solution from which Keilis-Borok arrived at his equation for the static displacement). The close agreement between the measured static displacement field and

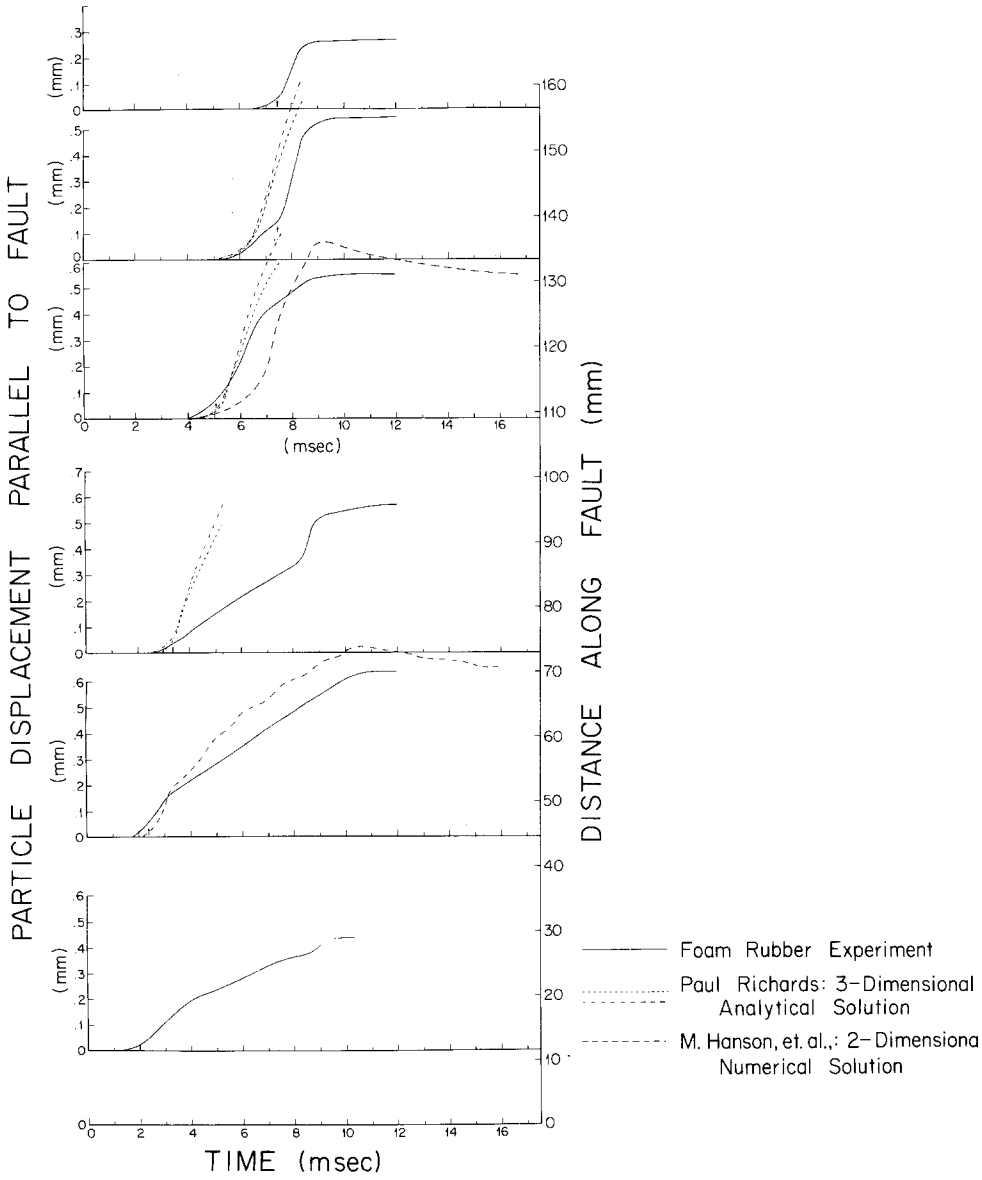

FIG. 6. See caption for Figure 5.

analytical results suggests that the stick-slip event we measured had a nearly constant stress drop over the fault plane.

Displacement-time functions for 12 points adjacent to the fault trace are shown in Figures 5 and 6. In both figures, the left ordinates measure the displacement in tenths of millimeters, the right ordinate gives the location of the particle with respect to one end of the fault trace in millimeters, and the abscissa gives the time in milliseconds. All of

these points are within 5 mm of the fault trace. In each case, we have drawn a smooth curve through the data. In addition to the results from our experiment, we plotted analytical results for the expanding circular fault (Richards, 1973) and results from a 2-D numerical model (Hanson, Sanford and Schaffer, 1974). Richards' (1973) results were obtained by using his computer program and numerically integrating the acceleration results for a self-similar, circular crack with a rupture velocity 0.75 β. We normalized

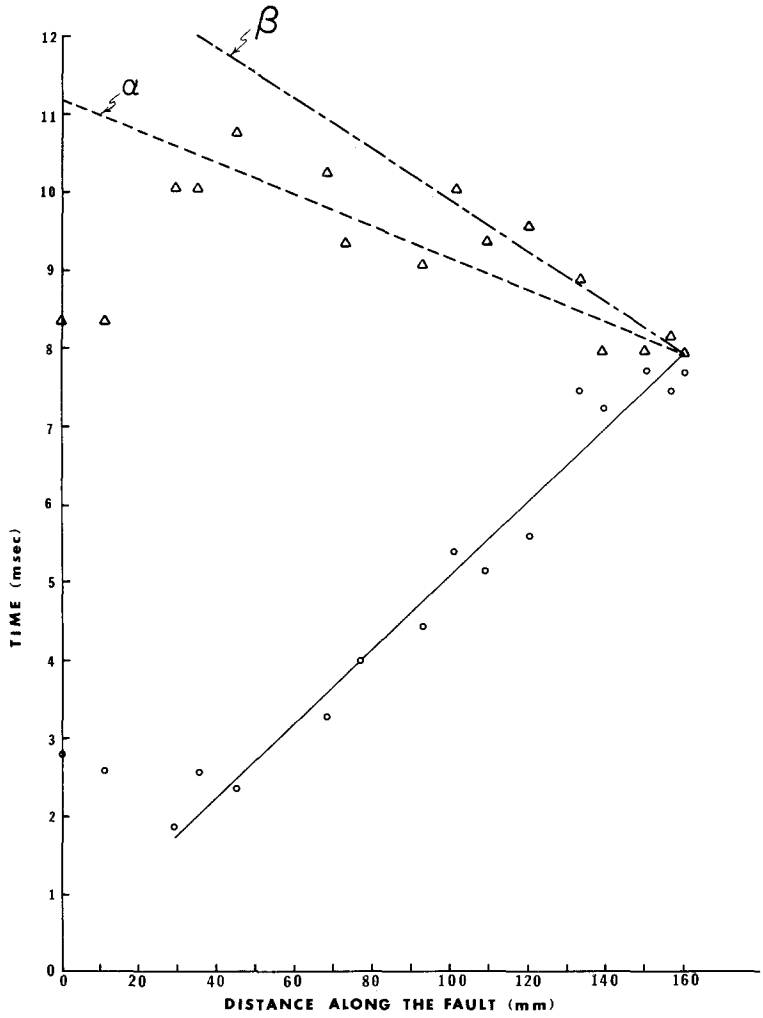

FIG. 7. Time of initiation of maximum particle velocity versus distance along the fault (shown as circles). The slope of line passing through circles is 0.7 β. Plotted as triangles is time at which particles attain their static values of displacement. Two dashed reference lines originate at 160 mm, one with slope of α, the other with β.

the results to stress drops of 0.0165 and 0.015 μ respectively (the higher stress drop giving the higher velocity curve). Because Richards' (1973) solution is self-similar, it is meaningful to compare only the initial part of the time function (before any edge effects occur). The curves from Hanson, Sanford and Schaffer (1974) are for a one-dimensional, unilaterally propagating and stopping shear crack with a rupture velocity of 0.69 β. We normalized their results so that the static displacement values for corresponding points are equal.

Examination of the displacement-time histories shows that the surface rupture originated about 30 mm from one end of the fault and then propagated bilaterally to both ends. Thus, the rupture propagated considerably longer in one direction than in the other. The characteristics of the wave form which delineate the passage of the rupture front are not known for certain, and thus, it is difficult to measure the rupture velocity with certainty. In order to estimate the time of passage of the rupture front, we selected the time of initiation of maximum particle velocity indicated by small arrows in Figures 5 and 6. In Kostrov's (1964) self-similar solution, a particle on the fault plane would initially experience an infinite particle velocity at the arrival time of the rupture front. Thus, it is not unreasonable to expect the first motion of a particle slightly off the fault would also experience its maximum velocity when the rupture front passed nearest to it. A graph of the time of initiation of maximum particle velocity plotted as a function of distance along the fault is shown in Figure 7. A least-squares fit to the data for distances beyond 30 mm gives a slope of 21 mm/msec (equivalent to 0.7 β). This is only the apparent velocity along the surface; if the rupture initiated at depth, the rupture velocity at depth could be as small as 0.63 β.

Perhaps the most prominent feature in Figures 5 and 6 is the increase in peak particle velocity (determined by measuring the slope of the displacement-time function) as the rupture propagates down the fault. A plot of estimated peak particle velocity (normalized by $\beta\Delta\tau/\mu$, the value of maximum particle velocity predicted by the simple formula of Brune, 1970) versus distance along the fault is shown in Figure 8. Estimating the peak particle velocity required considerable smoothing because of the high-frequency, digitization noise in the measurements. Hence, there is a possibility that we have smoothed over some high-velocity, high-frequency parts of the time function. We estimate the uncertainty in measurement of particle velocity for the larger values to be about 20 per cent. Near the initial surface rupture (between 30 and 40 mm along the fault), the peak particle velocity has a value of about 22 per cent of $\Delta\tau\beta/\mu$. Particles near the center of the fault experience maximum velocities of about 40 per cent of $\Delta\tau\beta/\mu$. The fact that the peak particle velocity for points near the center of the fault should be about one-half the value predicted by Brune's (1970) instantaneous stress pulse model is in agreement with results from the propagating circular fault (Kostrov, 1964; Kanamori, 1972; Brune, 1973; Abe, 1974). Between 120 and 150 mm along the fault, a very high particle velocity of 130 per cent of $\Delta\tau\beta/\mu$ is attained. We attributed this high value of particle velocity to a resonance caused by constructive interference of waves emanating from the boundary of the fault, because the distinct peak is preceded by a decrease as is typical of interference patterns. (The particles at 133 and 140 mm along the fault also show anomalous behavior in the plot of the apparent rupture velocity.) Maximum particle velocities for other points near the end of the fault have reached as high as 60 to 65 per cent of $\Delta\tau\beta/\mu$, which is approximately a threefold increase in peak particle velocity over the propagation path of approximately 130 mm.

Two physical processes may contribute to an increase in particle velocity in the direction of rupture propagation. First, any propagating source, such as a rupture front, will focus energy in the direction of propagation (Doppler focusing). Second, stress concentration can lead to high particle velocities in the immediate neighborhood of the crack tip. This is particularly true in some of the theoretical models which may constrain the rupture velocity in a nonphysical way. In our case, it is probable that most of the increase in particle velocity results from Doppler focusing. In a general way, the observed focusing is predicted by the theoretical models (Kostrov, 1970), and the numerical model (Hanson *et al.*, 1974). How important focusing will be during an earthquake will depend critically on the coherence of the seismic waves as the rupture propagates. A continuously

propagating rupture in a homogeneous medium could result in very high particle velocities.

Shown as triangles in Figure 7 are the estimated times at which particles adjacent to the fault attained their static values of displacement. The scatter in the data may stem from two sources. First, we cannot specify the precise moment when the static value is

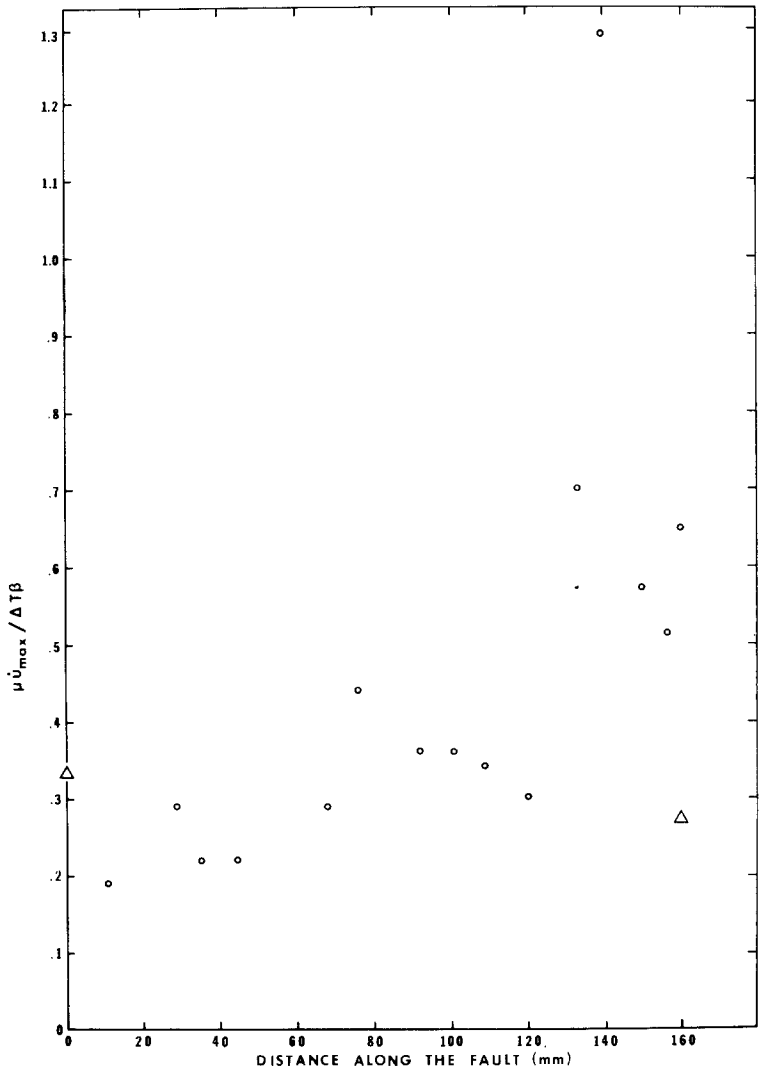

FIG. 8. Peak particle velocity normalized by $\Delta\tau\beta/\mu$ versus distance along the fault trace. Triangles shown at 0 and 160 mm are normalized maximum particle velocity values for normal component of displacement.

attained because of the shape in the time function and the errors in the data. Second, waves produced by stopping of the rupture on the boundary at depth may affect the locking of the fault. We cannot conclude from the data that the fault locked at either the *P*-wave or *S*-wave speed (equal to the slope of the respective dashed lines in Figure 7).

The values of static and dynamic displacement normal to the fault are much smaller than the corresponding values parallel to the fault. However, the maximum normal

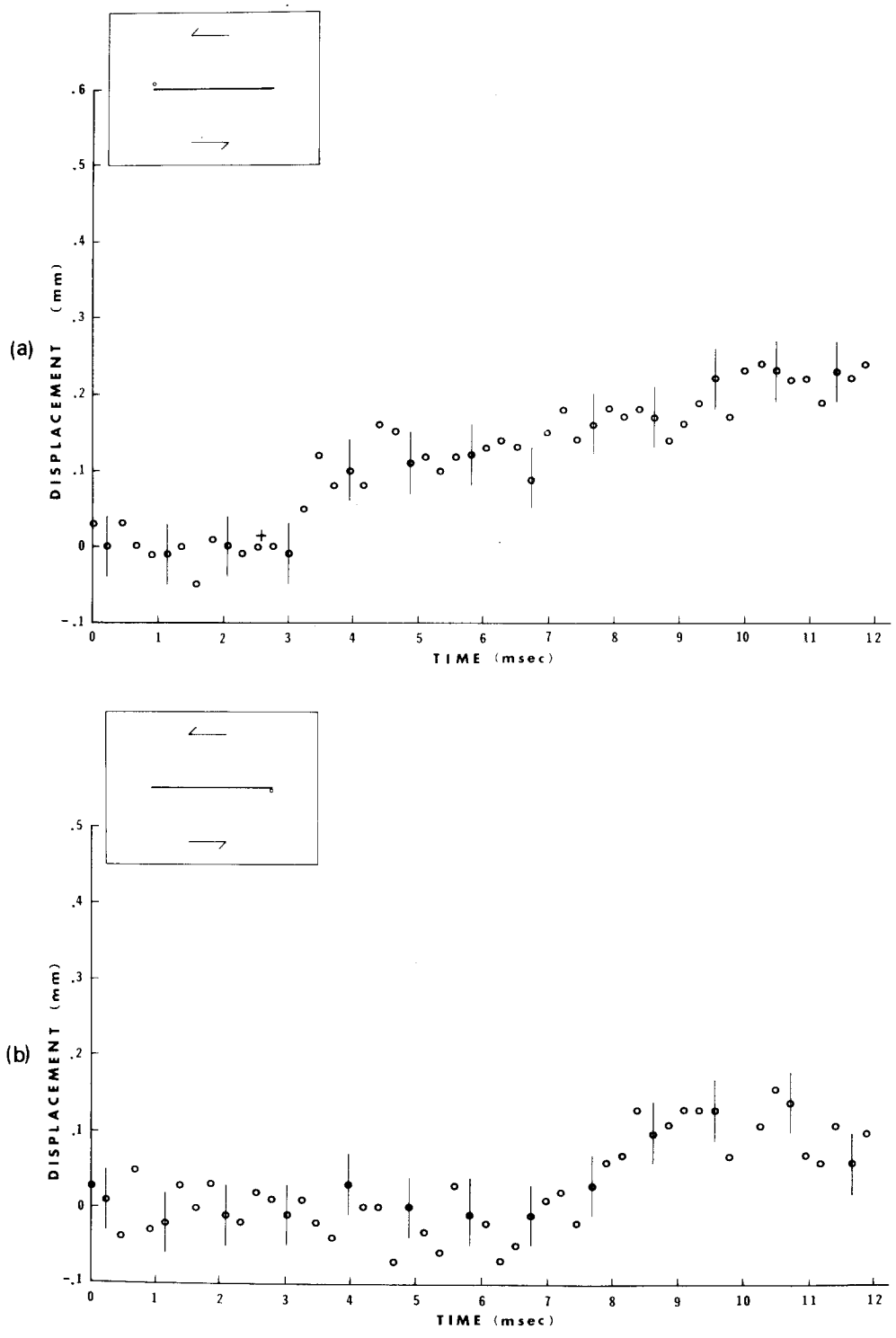

FIG. 9. The time history of displacement normal to the fault for points located at the ends of the fault are plotted. The *insert* in *upper left-hand corner* in (*a*) and (*b*) depicts the location of each particle, respectively. The rupture initiated near the end for the particle shown in (*a*).

particle velocities indicated by triangles in Figure 8 are comparable with the velocity of the parallel component near the center of the fault. The largest amplitudes for the normal component of displacement occurred at the ends (shown in Figure 9, a and b). The static values of 0.25 and 0.18 mm agree quite well with the theoretical value of 0.17 mm. None of the points, including those beyond the end of the fault, exhibit a dynamic displacement pulse normal to the fault like that seen on the Station 2 strong-motion instrument for the 1966 Parkfield earthquake (Hudson and Cloud, 1973; Aki, 1968). Within the accuracy of this experiment, the dynamic value of displacement normal to the fault never exceeds the static value, i.e., we have not observed any overshoot in the displacement-time functions such as that observed at Station 2 for the Parkfield earthquake.

Conclusions

1. The foam rubber experiment has been successfully used to study the elastodynamic response resulting from a propagating release of tractions over a plane.
2. The data illustrate the near-field focusing of energy in the direction of propagation.
3. The transverse motion at the ends of the fault has velocities comparable to the maximum velocity of the parallel component at the center of the fault, but at no point do the data exhibit a transverse displacement pulse similar to that observed at Station 2 for the 1966 Parkfield earthquake.
4. Agreement between analytical and numerical solutions for the elastodynamic near-field with the data from this experiment (e.g., focusing of energy) suggests that such solutions embody much of the physics associated with dynamic shear rupture on a prescribed plane.
5. Results of the type obtained in this experiment can be very important in the problem of microzonation for earthquakes, i.e., determining the probable values of peak particle velocity and acceleration at various sites near a fault.
6. This experiment was carried out on very limited funds and in no sense represents the optimum achievable results. Cameras with higher resolution are available. Our digitizing process was not optimum. Thus, although these results are very encouraging, we expect much better results in the future.

Acknowledgments

The authors are indebted to Paul Richards who generously allowed us to use his code KRACK which we used to compute displacements for the 3-D self-similar solution. The authors wish to thank Mr. Blake Barton of General Dynamics Corporation whose photographic expertise enabled us to perform this experiment. We would also like to thank Mr. Don Betts and Ms. Lucy Archuleta for drafting the figures. One of the authors (RJA) benefited greatly during this experiment from the continual support and advice of two of his colleagues, Messrs. Steven M. Day and Duncan C. Agnew. Keiiti Aki pointed out to the authors the importance of the result for transverse displacement at the end of the fault.

References

Abe, K. (1974). Fault parameters determined by near- and far-field data: The Wakasa Bay earthquake of March 26, 1963, *Bull. Seism. Soc. Am.* **64,** 1369–1382.

Aki, K. (1968). Seismic displacements near a fault, *J. Geophys. Res.* **73,** 5359–5376.

Brune, J. N. (1970). Tectonic stress and the spectra of seismic shear waves from earthquakes, *J. Geophys. Res.* **75,** 4997–5009.

Brune, J. N. (1971). (Correction) Tectonic stress and the spectra of seismic shear waves from earthquakes, *J. Geophys. Res.* **76,** 5002.

Brune, J. N. (1973). Earthquake modeling by stick-slip along pre-cut surfaces in stressed foam rubber, *Bull. Seism. Soc. Am.* **63,** 2105–2119.

Burridge, R. (1973). Admissible speeds for plane-strain self-similar shear cracks with friction but lacking cohesion, *Geophys. J.* **35,** 439–455.

Burridge, R. and C. Levy (1974). Self-similar circular shear cracks lacking cohesion, *Bull. Seism. Soc. Am.* **64,** 1789–1808.

Burridge, R. and J. Willis (1969). The self-similar problem of the expanding elliptical crack in an anisotropic solid, *Proc. Cambridge Phil. Soc.* **66,** 443–468.

Burridge, R. and G. S. Halliday (1971). Dynamic shear cracks with friction as models for shallow focus earthquakes, *Geophys. J.* **25,** 261–283.

Dieterich, J. H. (1973). A deterministic near-field source model, *Proc. World Conf. Earthquake Eng., 5th, Rome.*

Hanson, M. E., A. R. Sanford, and R. J. Shaffer (1974). A source function for a dynamic brittle unilateral shear fracture, *Geophys. J.* **38,** 365–376.

Hudson, D. E. and W. Cloud (1973). Seismological background for engineering studies of the earthquake, in *The Great Alaska Earthquake of 1964: Engineering*, National Academy of Sciences.

Kanamori, H. (1972). Determination of effective tectonic stress associated with earthquake faulting: The Tottori earthquake of 1943, *Phys. Earth Planet. Interiors* **5,** 426–434.

Keilis-Borok, V. I. (1959). On estimation of the displacement in an earthquake source and of source dimensions, *Ann. Geofis. (Rome)* **12** 205–214.

Kostrov, B. V. (1964). Self-similar problems of propagation of shear cracks, *J. Appl. Math. Mech.* **28,** 1077–1087.

Kostrov, B. V. (1966). Unsteady propagation of longitudinal shear cracks, *J. Appl. Math. Mech.* **30,** 1241–1248.

Kostrov, B. V. (1970). The theory of the focus for tectonic earthquakes, *Bull. Acad. Sci. USSR, Phys. Solid Earth* **4,** 258–267.

Madariaga, R. (1974). Seismic radiation from dynamic frictional faulting models, *EOS Trans. Am. Geophys. Union* **56,** 1147.

Neuber, H. (1958). (2nd ed.) Theory of notch stresses: Principles for exact calculation of strength with reference to structural form and material, (transl.) in *Kerbspannungslehre*, Springer-Verlag, Berlin, the Office of Tech. Info., AEC-tr-4547.

Reid, H. F. (1910). Mechanics of the earthquake, in *The California Earthquake of April 18, 1906, 2*: Carnegie Inst. of Washington, D.C. (updated in 1969).

Richards, P. G. (1973). The dynamic field of a growing plane elliptical shear crack, *Intern. J. Solids Struct.* **9,** 843–861.

Institute of Geophysics and Planetary Physics
Scripps Institution of Oceanography
University of California, San Diego
La Jolla, California 92037

Manuscript received April 11, 1975